NASA Technical Paper 1982

March 1982

Elastic-Plastic Finite-Element Analyses of Thermally Cycled Single-Edge Wedge Specimens

Albert Kaufman

NASA

NASA
Technical
Paper
1982

1982

Elastic-Plastic Finite-Element Analyses of Thermally Cycled Single-Edge Wedge Specimens

Albert Kaufman
Lewis Research Center
Cleveland, Ohio

NASA
National Aeronautics
and Space Administration

**Scientific and Technical
Information Branch**

Summary

Three-dimensional elastic and elastic-plastic stress-strain analyses using the MARC nonlinear, finite-element program were performed for single-edge wedge specimens subjected to thermal cycling in fluidized beds. Three different combinations of alloys and cycling conditions were analyzed to obtain the stress-strain-temperature histories at the critical locations for the purpose of developing a life prediction method.

Two alloys (NASA TAZ-8A and 316 stainless steel) were considered in this study. The cyclic condition used for the NASA TAZ-8A alloy was alternate 3-minute immersions in a cooling bed at 316° C and in a heating bed at 1088° C. The cyclic conditions used for the 316 stainless steel alloy were alternate 4-minute immersions in a cooling bed always maintained at 21° C and in a heating bed at a temperature of either 850° or 960° C.

Elastic analysis results from the MARC program for both alloys were in good agreement with previous results of elastic analyses that used the NASTRAN and ISO3DQ finite-element programs. The NASA TAZ-8A alloy exhibited no plastic strains, and the elastic and elastic-plastic analyses gave identical results throughout the thermal cycle. Elastic-plastic solutions at the critical locations for both 316 stainless steel alloy cyclic conditions demonstrated plastic strain reversal with a shift of the mean stresses in the compressive direction. The maximum equivalent total strain ranges at the critical locations were 13 to 22 percent greater than that calculated from the elastic analyses. Increasing the heating bed temperature from 850° to 960° C doubled the maximum equivalent plastic strain and increased the maximum equivalent total strain range for the cycle by about 25 percent.

Introduction

Hot-section components of aircraft gas turbine engines, such as combustor liners and turbine blades and vanes, are subject to cyclic thermomechanical loading, which can result in progressive fatigue damage and eventual cracking. Life prediction methods to assess the durability of these components have been under development at the NASA Lewis Research Center and are discussed in references 1 to 6. To apply these methods, it is first necessary to determine the temperature-stress-strain history of the part.

As part of the life prediction studies at Lewis, single-edge wedge specimens have been thermally cycled in fluidized beds as described in reference 7. In these tests fluidized beds were used to rapidly heat and cool prismatic bar specimens of wedge cross section. The bars were tested so that they failed by thermal fatigue cracking. Elastic stress-strain histories at the critical edge locations of these specimens were obtained by performing three-dimensional finite-element structural analyses under a joint NASA Lewis–Air Force program. Lewis used the NASTRAN computer program (ref. 8); the Air Force Aero Propulsion Laboratory used the ISO3DQ computer program (ref. 9). The results of these elastic analyses are reported in reference 10.

Nonlinear finite-element computer programs such as MARC (ref. 11) are available for more rigorous three-dimensional cyclic analyses of components involving inelastic plastic and creep strains. These programs have had some limited use as research analytical tools, as in the turbine blade airfoil studies described in references 12 to 14. However, nonlinear programs have not been applied to the design of engine hot-section parts mainly because of the extensive demands they make on computer resources and because of inadequacies in both cyclic property data for superalloy materials and the current state of transient heat transfer analysis methods. The NASA Lewis Research Center has instituted a program to improve the quality of the material property and temperature input for nonlinear structural analyses.

This study was conducted to determine the elastic-plastic stress-strain histories at the critical locations for single-edge wedge specimens that were thermally cycled in fluidized beds. These analytical results are required, in conjunction with experimental failure data, in the development and evaluation of life prediction methods at Lewis. The results of similar MARC elastic-plastic structural analyses for double-edge wedge specimens that were also thermally cycled in fluidized beds are reported in reference 15.

The structural analyses were performed with the MARC nonlinear, finite-element program using a combined isotropic-kinematic hardening model described in reference 11. The specimen geometry was modeled with 20-node, isoparametric, three-dimensional elements. Three cases involving two alloys (NASA TAZ-8A specimens under one cycling condition and 316 stainless steel specimens under two cycling conditions) were studied. The test condition for which NASA TAZ-8A alloy was analyzed was for alternate 3-minute immersions

in fluidized beds maintained at 316° and 1088° C. The 316 stainless steel alloy specimens were analyzed for 4-minute alternate immersions in fluidized beds maintained at 21° C and either 850° or 960° C. Elastic and elastic-plastic solutions from the MARC program were compared for the same alloys, geometry, and thermal cycling conditions. In addition, to verify the analyses as much as possible, elastic results from MARC were compared with the elastic analysis solutions from the NASTRAN and ISO3DQ programs given in reference 10.

Analytical Procedure

Elastic-plastic stress-strain states were calculated for single-edge wedge specimens of three combinations of alloys and fluidized-bed cycling conditions. The alloys and test conditions for the three cases studied are presented in table I. Alloy compositions are given in reference 16.

Input for Analyses

The specimen geometry, material properties, and thermal loading that were used as input to the structural analyses are described in this section.

Geometry. – The geometry of the single-edge wedge specimen is illustrated in figure 1. To be consistent with the NASTRAN and ISO3DQ analyses of reference 10, the leading-edge radius was "squared off" to 1.02 millimeters for the finite-element model.

Material properties. – The physical properties of the alloys, which were obtained from reference 10, are detailed in table II. An elastic-plastic analysis requires, in addition, mechanical properties to define the work-hardening behavior under plastic straining; these data were obtained from reference 16 and are given in table III. Since the MARC program requires instantaneous coefficients of thermal expansion, the mean coefficient data in table II were converted to instantaneous values for input.

Thermal loading. – The transient temperature loading on the single-edge wedges was determined from thermocouple data. Calibration specimens of the two alloys were instrumented chordwise at the midspan with five embedded thermocouples and cycled in the fluidized beds (schematically shown in fig. 2). The locations of the thermocouples at the wedge cross section are shown in figure 3. The Inconel 600 sheathed Chromel-Alumel thermocouples were mounted in grooves milled in the surface of the specimen and secured by a ceramic cement. The grooves were 0.56 millimeter wide and 0.5 millimeter deep. Other details of the installation and procedure are given in reference 7. The thermocouple outputs were cross-plotted to give temperatures of the midchord at the midspan at various time increments after immersion into the fluidized beds. These data, taken from reference 10, are reproduced in figure 3 for the three cases analyzed. It was assumed that there was no temperature gradient through the thickness of the wedge.

Another set of thermocuple data was taken with five thermocouples mounted along the leading edge over half the span. These data revealed a longitudinal (along the span of the specimen) temperature gradient that varied with the different time increments. The maximum variation was about 16 percent greater at the ends of the wedge than at the midspan and occurred after 30 seconds of heating. However, for any one time increment the ratio of the leading-edge midspan temperature to that of any other span location was nominally the same for all the cases. A least-squares best-fit parabola was determined for each time increment and these data, taken from reference 10, are reproduced in table IV. This parabolic temperature variation along the span was assumed over the complete chord of the wedge.

The temperatures at midspan were determined from the appropriate plot in figure 3. For locations other than midspan the temperatures were determined by using the midspan temperature modified by the values given in table IV. Therefore the temperature distribution at any point of the wedge was determined from figure 3 and table IV.

Methods of Analysis

Elastic and elastic-plastic stress-strain distributions in the wedge specimens were calculated from the MARC nonlinear, finite-element computer program. Computations were performed for the time increments into which the thermal cycle was subdivided, as shown in figure 3. There were 34 time increments (17 heating, 17 cooling) for the NASA TAZ-8A cycle and 42 time increments (21 heating, 21 cooling) for the 316 stainless steel cycles. Elastic solutions using MARC were compared with the NASTRAN and ISO3DQ analyses of reference 10 in order to check the program input and the finite-element model. The elastic analyses were performed by setting the material yield strength to a fictitiously high level. The elastic-plastic analyses only had to be carried out for two cycles in order to attain reasonably stable stress-strain hysteresis loops. Stability was indicated when the cooling part of the hysteresis loop for the second cycle essentially coincided with the cooling part of the hysteresis loop for the first cycle.

Plasticity computations, which were based on incremental plasticity theory, used the von Mises yield criterion and normality flow rule. The yield surface under reversed loading was found from the monotonic stress-strain behavior in conjunction with a combined isotropic-kinematic hardening model. A preprocessor program converted the thermal loading data from the wedge

specimen into the form of a sixth-order polynomial equation. A subroutine inserted into MARC interpolated from these equations for the local temperatures at the Gaussian integration points in the finite-element model. Another subroutine inserted into MARC inputted the stress-strain properties as functions of temperature and determined the yield stresses and work-hardening slopes for the local temperatures at the Gaussian integration points.

Outputs from the program were the effective normal and shear stresses, the equivalent total and plastic strains, the normal and shear total and plastic strains, the principal stresses and strains, and the nodal displacements. Stress and strain outputs were given for the Gaussian integration points. To prevent excessive generation of computer printout, the output was restricted to high-strain regions and some other locations required for comparison with the results of reference 10. Contour plots of effective stress, longitudinal stress and total strain, equivalent plastic strain, and temperature were obtained for the time increments of maximum and minimum strain in the cycle.

Approximately 17 hours of execution time per cycle on a Univac 1110/42 computer system was required to run these problems. If some of the time increments were condensed, it should be possible to perform an elastic analysis over the cycle with about an order of magnitude less computer time than was necessary for a two-cycle elastic-plastic analysis.

Finite-Element Model

The finite-element model is illustrated in figure 4. Only one-fourth of the wedge specimen needed to be modeled because of symmetry; this model was the volume enclosed by the surface and intersecting midchord and midspan planes of symmetry. The element used was a 20-node, isoparametric, three-dimensional block with 8 corner nodes and 12 edge midpoint nodes. This element had 27 Gaussian integration points. The model consisted of 30 of these elements with a total of 268 nodes and 662 unsuppressed degrees of freedom.

To maintain symmetry, all nodes initially on the midspan and midchord faces of the model were constrained to lie on the midspan and midchord planes, respectively. In addition, one node at the leading edge was constrained chordwise (leading to trailing edge) in order to prevent rigid-body motion in that direction.

Results and Discussion

The results of the MARC elastic and elastic-plastic analyses of thermally cycled single-edge wedge specimens of NASA TAZ-8A and 316 stainless steel alloys are discussed herein. Elastic results from MARC are compared with results of ISO3DQ and NASTRAN analyses taken from reference 10. MARC elastic and elastic-plastic stress-strain histories are then compared for each case at the critical location (the location where the maximum total strain range occurred). Finally, MARC elastic-plastic results are compared for the two 316 stainless steel alloy cases.

Comparison of Elastic Analyses

Elastic analyses using MARC were performed by treating each of the time increments into which the thermal cycle was subdivided as separate steady-state conditions. Figures 5 and 6 show a comparison of MARC results with the results of similar elastic analyses using ISO3DQ and NASTRAN that are taken from reference 10 for the same alloys, geometry, and thermal cycling increments. The finite-element models in order from finest to coarsest were the NASTRAN model with 192 solid, 8-node elements, the MARC model with 30 solid, 20-node elements, and the ISO3DQ model with 24 solid, 12-node elements. The MARC results shown in figures 5 and 6 apply to locations close to the span positions indicated in the figures but not exactly at those span positions because of differences in the finite-element models and in program output modes.

In figure 5 stress solutions from NASTRAN, ISO3DQ, and MARC are compared for NASA TAZ-8A alloy after 15 seconds into the heating part of the cycle. Longitudinal stresses are shown along the midchord at one-quarter span, which was approximately the critical span location for this case. The results from the three programs are in good agreement. As expected, the relatively hot leading edge was in compression.

In figure 6, longitudinal stresses calculated from ISO3DQ and MARC at the critical locations (based on ISO3DQ analyses) are shown as a function of cycle time for each case. The highest compressive stresses were reached during the first 30 seconds of heating, and the highest tensile stresses during the first 15 seconds of cooling. The results of figure 6 demonstrate generally good agreement between the computed elastic analysis results from ISO3DQ and MARC.

Comparison of MARC Elastic and Elastic-Plastic Analyses

The results of the MARC elastic and elastic-plastic analyses are presented in figure 7 for each of the three cases in terms of the effective stress–equivalent total strain response at the critical location. In order to construct the stress-strain hysteresis loops from the effective stresses and equivalent strains, which are always calculated as positive values, signs were assigned based on those of the principal stresses or strains with the greatest magnitude at the time increment under

consideration. Critical locations shown in figure 7 were only approximate since the total strains were relatively constant over a large region of the leading edge. Elastic-plastic analyses were continued for two cycles in order to eliminate from consideration the nonrecurring plastic strains on initial heating and to attain reasonably stable solutions. Elapsed times during the heating and cooling phases of the thermal cycle are also shown in figure 7.

As expected the leading edge went into compression during the heating part of the cycle, reaching minimum strains after about 9 seconds immersion in the heating bed. As the metal temperatures approached equilibrium, the strains increased and rapidly became tensile during the cooling part of the cycle. Maximum strains occurred after 9 to 15 seconds immersion in the cooling bed. The elastic-plastic analysis of the NASA TAZ-8A alloy (fig. 7(a)) did not indicate the presence of plastic strains anywhere in the finite-element model, and the stress-strain solutions were identical to those from the elastic analysis throughout the cycle. The elastic-plastic analyses for the 316 stainless steel alloy cases (figs. 7(b) and (c)) exhibited compressive plastic strains at the critical location during heating and tensile plastic strain reversal during cooling. These plastic strains caused the hysteresis loops to shift under cycling, as shown in figures 7(b) and (c).

Equivalent total strain ranges and mean effective stress levels from the hysteresis loops of figures 7(b) and (c) are summarized in figure 8 in bar graph form for convenience of comparison. The total strain ranges shown in figure 8(a) for the 316 stainless steel alloy at the critical locations were 13 and 22 percent greater for the low- and high-temperature cases, respectively, than those computed from elastic analyses. The relatively large discrepancy in total strain ranges obtained from the two types of analysis was primarily caused by the difference between the low yield strength of the 316 stainless steel alloy and the maximum elastically computed stresses. This difference is particularly noticeable in figure 7(c) for case 3, where tensile elastic stresses were calculated that were approximately four times the yield strength in reversed tension. In both cases elastic-plastic analyses demonstrated a significant shift of the mean stress in the compressive direction and relatively wide stress-strain hysteresis loops. Figure 8(b) shows that the compressive mean stress for the 850° C heating bed temperature more than doubled after two cycles of repeated plastic straining as compared with the elastic results. For the 960° C heating bed temperature the elastic analysis indicated a tensile mean stress, but the elastic-plastic analysis showed a compressive mean stress during the second cycle.

Comparison of Elastic-Plastic Results for Alloy Cases

Temperature-stress-strain distributions over the specimen midchord plane are displayed for the three cases in figure 9 at the time of minimum total strain and in figure 10 at the time of maximum total strain. The contour plots of temperature, effective stress, longitudinal stress and total strain, and equivalent plastic strain were obtained from the elastic-plastic analyses during the second thermal cycle. Since NASA TAZ-8A alloy exhibited no plastic strains, equivalent plastic strain contours are presented only for the 316 stainless steel alloy.

The temperature-stress-strain distributions shown in figures 9 and 10 indicate approximately uniform conditions at the leading edge in the upper half of the model. This uniformity is not quite so evident in figures 9(d) and 10(d) because the longitudinal total strains include thermal deformation components. The relative uniformity of the temperatures, stresses, and strains over a large region of the leading edge suggests that cracks could occur anywhere in this region because of variations in temperature and material properties. Therefore these studies cannot be used to substantiate the ability to predict crack initiation location.

The critical location computed from the MARC analyses occurred about one-quarter span along the leading edge for all three cases (fig. 7). This location is essentially in agreement with the critical location computed from the ISO3DQ analyses for the NASA TAZ-8A and high-temperature 316 stainless steel cases (figs. 6(a) and (c)). There was a small discrepancy between the MARC and ISO3DQ programs in the critical location predicted for the low-temperature 316 stainless steel alloy case (fig. 6(b)).

The highest equivalent plastic strain occurred at the time of maximum total strain during cooldown. A comparison of the equivalent plastic strain contours of figure 10(e) shows that increasing the fluidized heating bed temperature from 850° C to 960° C for the 316 stainless steel alloy approximately doubled the maximum plastic strains. From figure 8(a) it can be seen that increasing the heating bed temperature increased the maximum equivalent total range by about 25 percent. The maximum total strain ranges calculated for the single-edge wedge specimens were smaller than those reported for the double-edge specimens in reference 15 for test conditions similar to the high-temperature 316 stainless steel alloy case.

In assessing the analytical results it should be understood that the accuracies of the elastic-plastic analyses are susceptible to inadequacies in the input data, particularly in the material mechanical properties and constitutive relations. NASA Lewis is currently engaged in a program to improve the quality of the input data required for nonlinear structural analyses. The results of this study will be used to develop a life analysis system in which cyclic lives of complex structures can be determined from laboratory tests of simple specimens by

duplicating, in the specimen, the computed temperature-stress-strain history at the critical location of the structure. These results will also be used as input into various low-cycle-fatigue damage models in order to evaluate the applicability of different life prediction methods to structures with multiaxial stress-strain states.

Summary of Results

Three-dimensional finite-element analyses using the MARC nonlinear, structural computer program were performed for single-edge specimens thermally cycled in fluidized beds. The alloys and conditions were NASA TAZ-8A subjected to alternate 3-minute immersions in beds at 316° and 1088° C and 316 stainless steel subjected to alternate 4-minute immersions in beds at 21° C and either 850° or 960° C. The major results of this study were as follows:

1. Maximum equivalent total strain ranges calculated at the critical locations from elastic-plastic analyses for two cases involving the 316 stainless steel alloy were 13 to 22 percent greater than those calculated from elastic analyses. This discrepancy was mainly due to the large difference between the maximum elastically computed stresses and the yield strength of the alloy, particularly in reversed tension, which also resulted in relatively wide stress-strain hysteresis loops.

2. Mean effective stresses calculated at the critical location from elastic-plastic analyses for the 316 stainless steel alloy cases showed a significant shift in the compressive direction as compared with results of elastic analyses.

3. Plastic strain reversal was exhibited at the critical locations for the 316 stainless steel alloy cases. Increasing the fluidized heating bed temperature from 850° to 960° C doubled the maximum equivalent plastic strain and increased the maximum equivalent total strain range by about 25 percent.

4. Elastic-plastic analysis of the NASA TAZ-8A alloy case showed no plastic strains, and the stress-strain results throughout the cycle were identical with elastic analysis results.

5. Comparisons of MARC elastic analysis results with previously reported analytical results using NASTRAN and ISO3DQ were in generally good agreement even though the finite-element models were substantially different.

Lewis Research Center
National Aeronautics and Space Administration
Cleveland, Ohio, February 12, 1981

References

1. Hirschberg, M. H.; and Halford, G. R.: Use of Strainrange Partitioning to Predict High-Temperature Low-Cycle Fatigue Life. NASA TN D-8072, 1976.
2. Saltsman, J. F.; and Halford, G. R.: Application of Strainrange Partitioning to the Prediction of Creep-Fatigue Lives of AISI Types 304 and 316 Stainless Steel. J. Pressure Vessel Technol., vol. 99, no. 2, May 1977, pp. 264-271.
3. Hirschberg, M. H.; and Halford, G. R.: Strainrange Partitioning—A Tool for Characterizing High-Temperature Low-Cycle Fatigue. NASA TM X-71691, 1975.
4. Halford, G. R.; Saltsman, J. F.; and Hirschberg, M. H.: Ductility Normalized-Strainrange Partitioning Life Relations for Creep-Fatigue Life Predictions. NASA TM-73737, 1977.
5. Manson, S. S.; Halford, G. R.; and Hirschberg, M. H.: Creep Fatigue Analysis by Strain-Range Partitioning. Design for Elevated Temperature Environment. S. Y. Zamrik, ed., American Society of Mechanical Engineers, 1971, pp. 12-24.
6. Spera, D. A.; and Grisaffe, S. J.: Life Prediction of Turbine Components: On-Going Studies at the NASA Lewis Research Center. NASA TM X-2664, 1973.
7. Bizon, P. T.; and Spera, D. A.: Comparative Thermal Fatigue Resistances of Twenty-Six Nickel- and Cobalt-Base Alloys. NASA TN D-8071, 1975.
8. The NASTRAN User's Manual (Level 16.0 Supplement). NASA SP-222(03), 1976.
9. User's Manual—Programs MESH3, ISO3DQ, and PROUT3 Turbine Engine Components Stress Simulation Program. Rept. 74-210860(2)-1A, AiResearch Mfg. Co., Mar. 1977.
10. Bizon, P. T.; et al.: Three-Dimensional Finite-Element Elastic Analysis of a Thermally Cycled Single-Edge Wedge Geometry Specimen. NASA TM-79026, 1979.
11. MARC General Purpose Finite Element Analysis Program. User Manual, Vols. A and B, MARC Analysis Research Corporation, 1979.
12. Kaufman, A.; and Gaugler, R. E.: Cyclic Structural Analyses of Air-Cooled Gas Turbine Blades and Vanes. SAE Paper 760918, Nov. 1976. (Also NASA TM X-73494, 1976.)
13. Kaufman, A.; and Gaugler, R. E.: Nonlinear, Three-Dimensional Finite-Element Analysis of Air-Cooled Gas Turbine Blades. NASA TP-1669, 1980.
14. Kaufman, A.: Comparison of Elastic and Elastic-Plastic Structural Analyses for Cooled Turbine Blade Airfoils. NASA TP-1679, 1980.
15. Kaufman, A.; and Hunt, L. E.: Elastic-Plastic Finite-Element Analyses of Thermally Cycled Double-Edge Wedge Specimens. NASA TP-1973, 1982.
16. Fritz, L. J.; and Koster, W. P.: Tensile and Creep Rupture Properties of (16) Uncoated and (2) Coated Engineering Alloys at Elevated Temperatures. (Rept.-931-21300, Metcut Research Associates, Inc.; NASA Contract NAS3-18911). NASA CR-135138, 1977.

TABLE I. - ALLOYS AND CONDITIONS ANALYZED

Alloy	Heating	Cooling	Immersion time in each bed, sec
	Fluidized-bed temperatures, °C		
NASA TAZ-8A	1088	316	180
316 Stainless steel	850	21	240
	960	21	240

TABLE II. - ALLOY PHYSICAL PROPERTIES

Temperature, °C	NASA TAZ-8A		316 Stainless steel	
	Modulus of elasticity, E, MN/m^2	Mean coefficient of thermal expansion from room temperature to indicated temperature, α, m/m °C	Modulus of elasticity, E, MN/m^2	Mean coefficient of thermal expansion from room temperature to indicated temperature, α, m/m °C
-17.8	208×10^3	10.3×10^{-6}	199×10^3	15.3×10^{-6}
37.8	206	10.6	197	15.5
93	205	11.0	194	15.7
149	205	11.5	190	15.9
204	203	11.9	186	16.2
260	202	12.1	181	16.6
316	201	12.1	177	16.9
371	199	12.2	172	17.3
427	198	12.4	166	17.6
482	197	12.6	162	18.0
538	194	12.8	157	18.4
593	192	12.8	152	18.5
649	190	13.0	145	18.5
704	187	13.1	139	18.7
760	183	13.3	137	18.9
816	178	13.5	132	19.0
871	168	13.9	130	19.1
927	146	14.2	128	19.2
982	139	14.6	126	19.3
1038	133	14.9	124	19.4
1093	128	15.3	123	19.4
Poisson's ratio	0.317		0.289	

TABLE III. - ALLOY MECHANICAL PROPERTIES

Alloy	Temperature, ^{o}C	Ultimate strength, MN/m^2	0.02-Percent yield strength, MN/m^2	0.2-Percent yield strength, MN/m^2	Reduction in area, percent
NASA TAZ-8A	21	993	689	821	6
	850	848	538	745	6
	925	648	338	517	7
	1000	469	234	365	11
316 Stainless steel	21	627	159	234	82
	593	441	76	103	71
	704	269	76	110	64
	816	159	76	103	87

TABLE IV. - TEMPERATURE VARIATION ALONG SPAN

[$T_{x,z} = T_{x,ms}\,(Az^2 + Bz + C)$, where $T_{x,z}$ is the temperature at any x, z coordinate (fig. 4), $T_{x,ms}$ is the temperature at the x coordinate at midspan, and z is the span coordinate; all temperatures in ^{o}F ($F = 9/5\ C + 32$).]

Time increment, sec	Heating bed			Cooling bed		
	A	B	C	A	B	C
0	-0.00870	0.0517	0.9205	-0.00666	0.03957	0.9427
3	.04401	-.2614	1.3891	-.01775	.1055	.8447
6	.03739	-.2221	1.3290	-.02384	.1416	.7911
9	.03688	-.2191	1.3372	-.02548	.1514	.7786
12	.03806	-.2261	1.3344	-.02731	.1622	.7622
15	.03695	-.2195	1.3300	-.02889	.1716	.7480
30	.02758	-.1638	1.2504	-.03047	.1810	.7338
45	.01769	-.1051	1.1630	-.03141	.1866	.7224
60	.01432	-.08506	1.1324	-.03442	.2044	.6905
75	.01006	-.05978	1.0934	-.03265	.1939	.7093
90	.00833	-.04948	1.0791	-.02867	.1703	.7440
105	.00557	-.03311	1.0528	-.02445	.1452	.7843
120	.00627	-.03722	1.0571	-.02276	.1352	.7981
135	.00440	-.02614	1.0415	-.01876	.1142	.8323
150	.00371	-.02205	1.0357	-.01533	.09107	.8622
165	.00297	-.01762	1.0285	-.01278	.07593	.8832
180	.00262	-.01553	1.0243	-.01212	.07198	.8876
195	↓	↓	↓	↓	↓	↓
210						
225						
240						

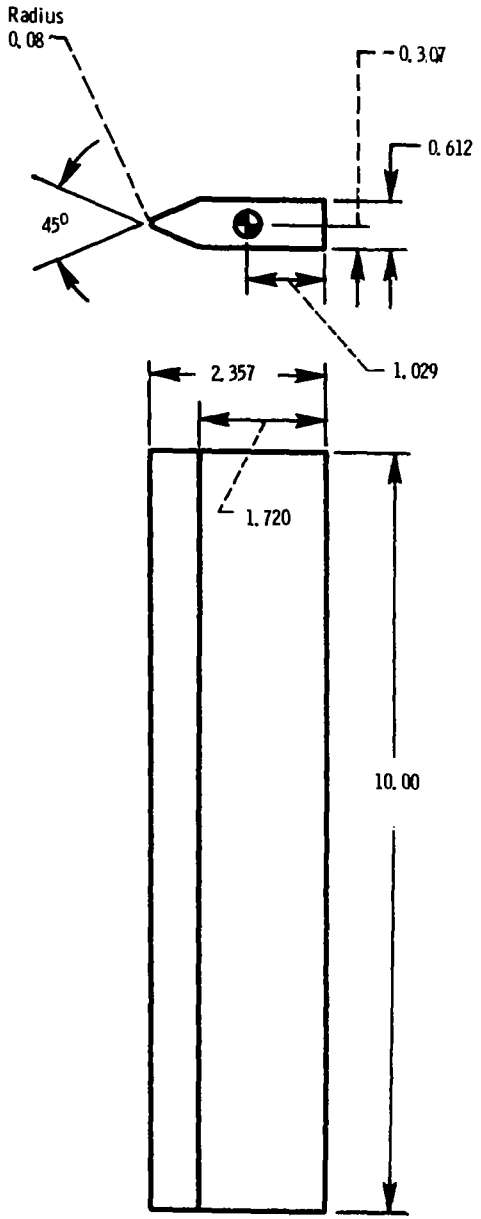

Figure 1. - Single-edge wedge geometry. (All linear dimensions are in centimeters.)

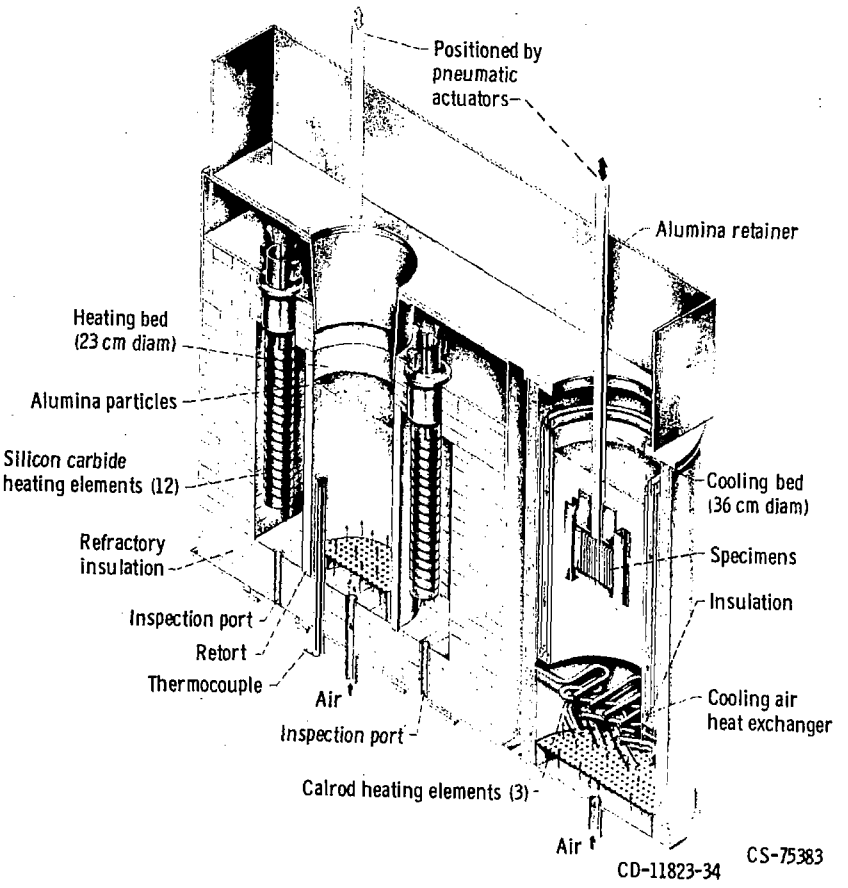

Figure 2. - Schematic of fluidized-bed test facility.

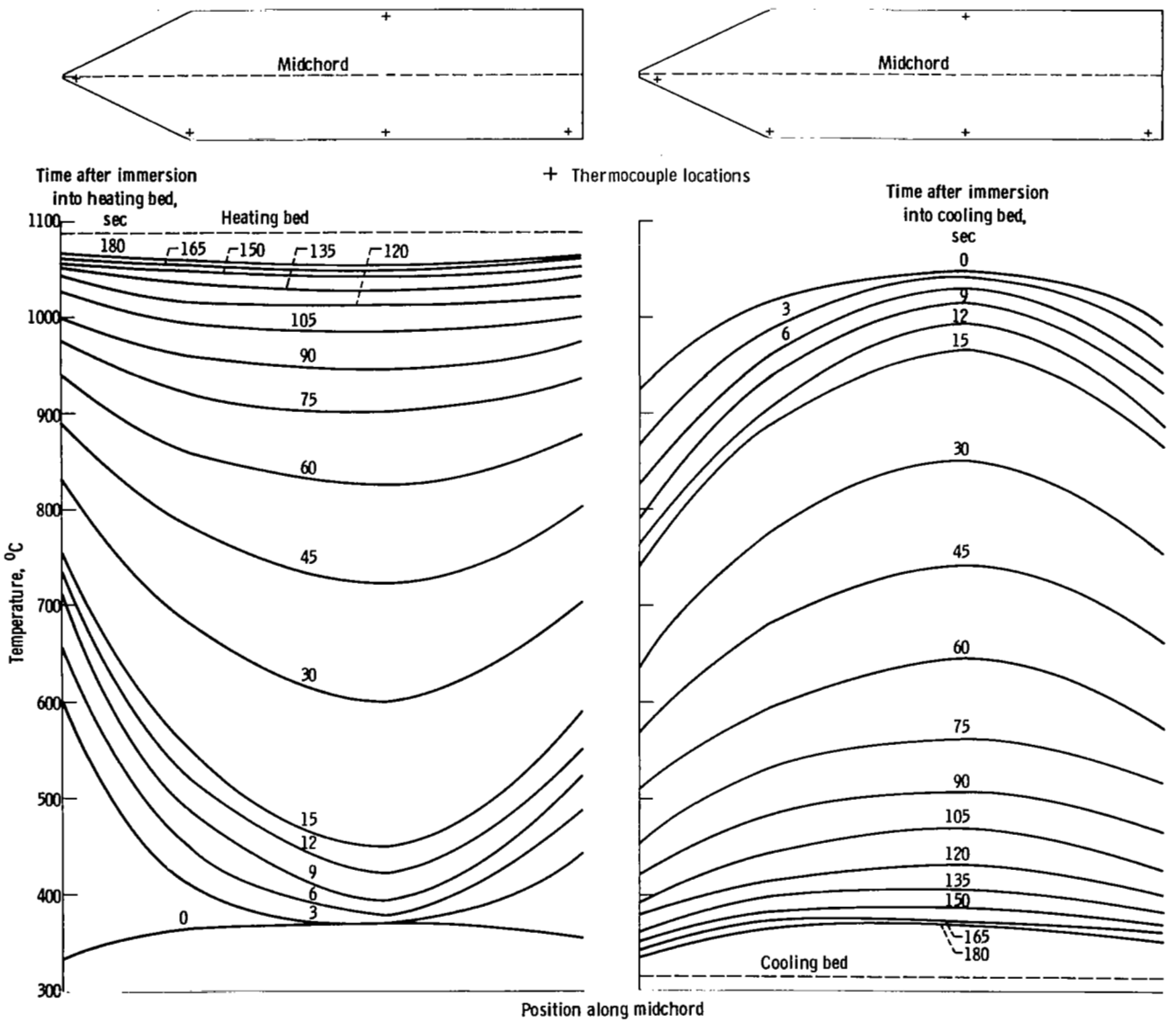

(a) NASA TAZ-8A alloy with fluidized beds maintained at 1088° and 316° C.

Figure 3. - Temperature of midchord at midspan at various times after immersion into the fluidized beds.

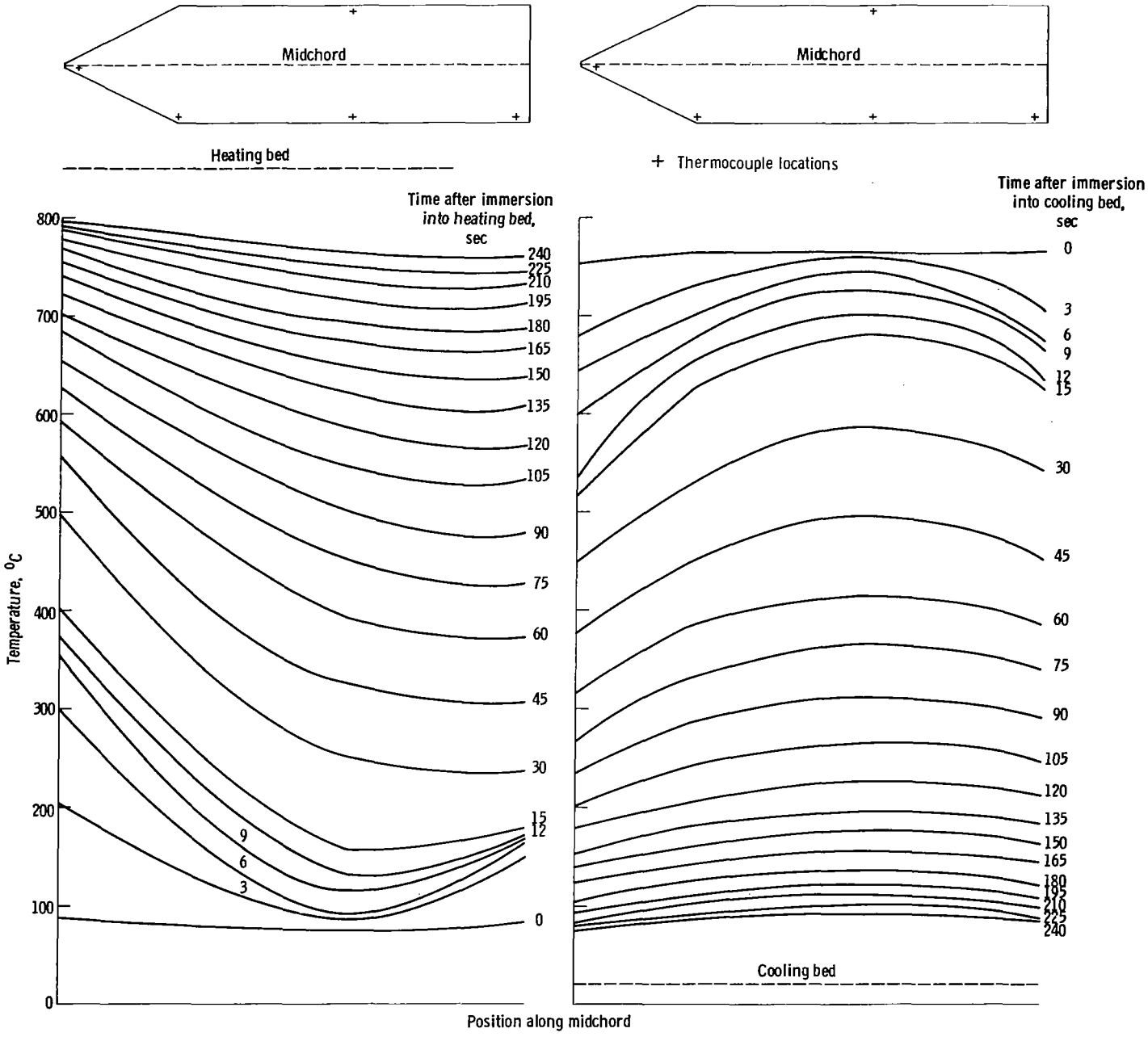

(b) 316 Stainless steel alloy with fluidized beds maintained at 850° and 21° C.

Figure 3. - Continued.

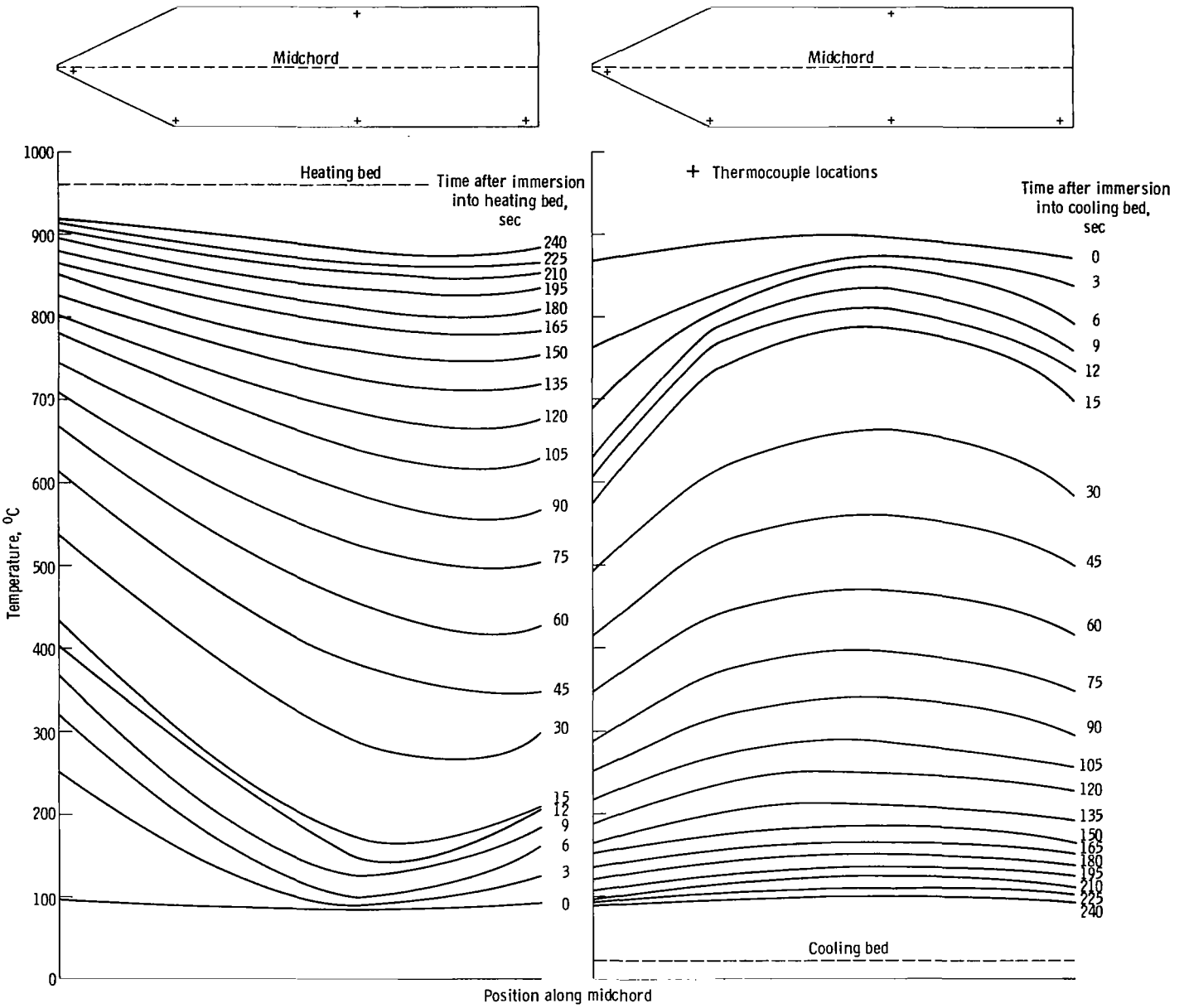

(c) 316 Stainless steel alloy with fluidized beds maintained at 960° and 21° C.

Figure 3. - Concluded.

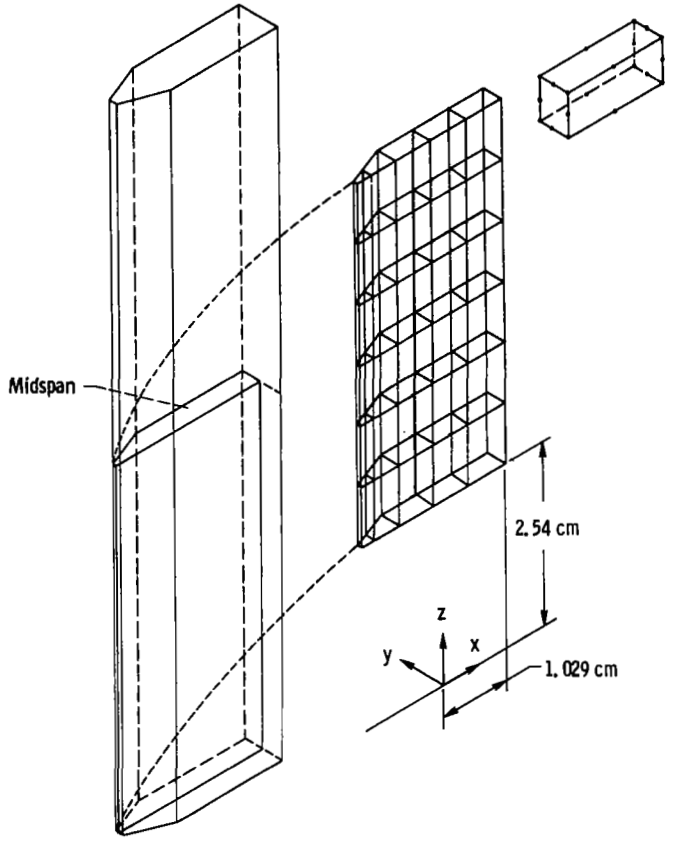

Figure 4. - Model and typical element used for MARC analysis with coordinate convention.

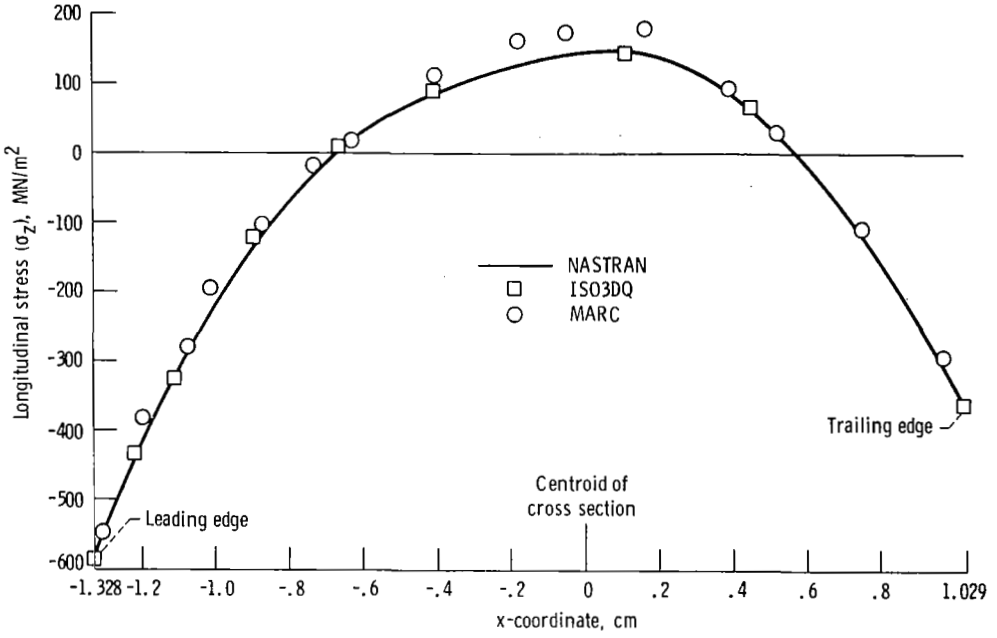

Figure 5. - Comparison of elastic results using MARC, ISO3DQ, and NASTRAN computer programs for NASA TAZ-8A alloy after 15 seconds of heating.

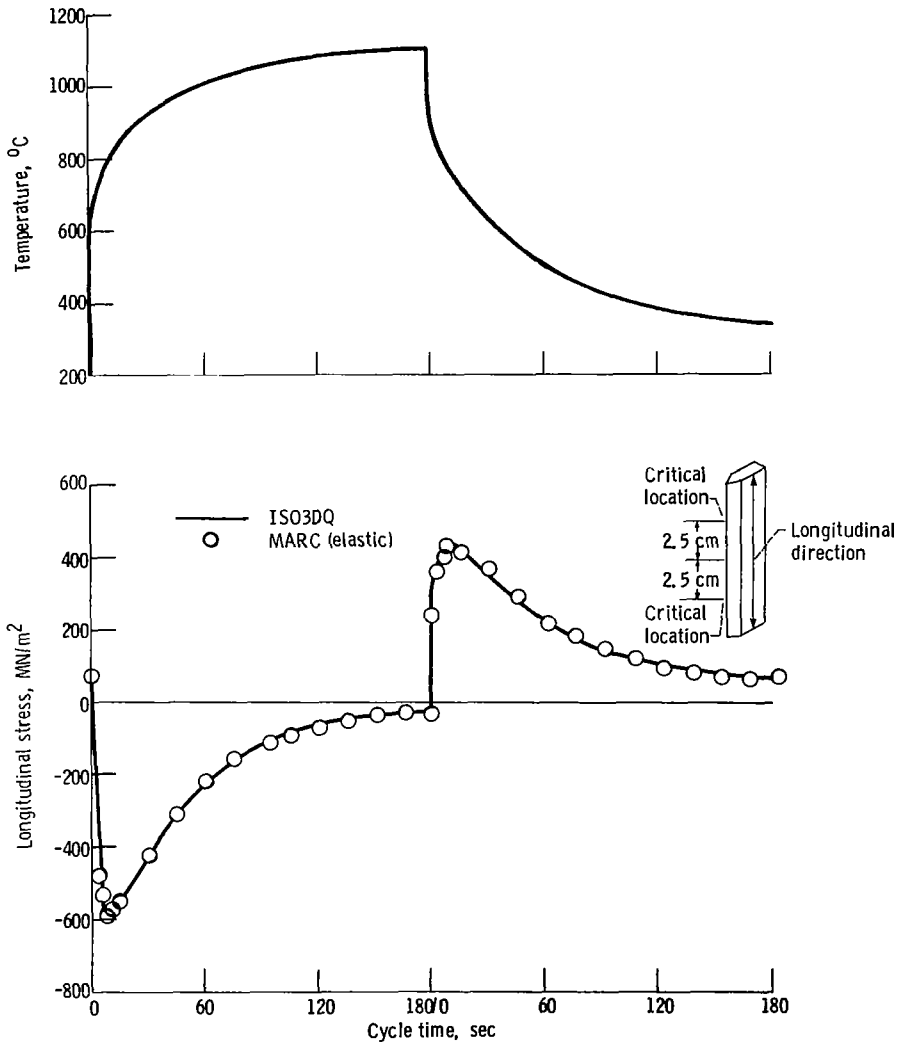

(a) NASA TAZ-8A alloy with the fluidized beds maintained at 1088° and 316° C.

Figure 6. - Comparisons of elastic results using MARC and ISO3DQ computer programs at critical locations during a typical thermal cycle.

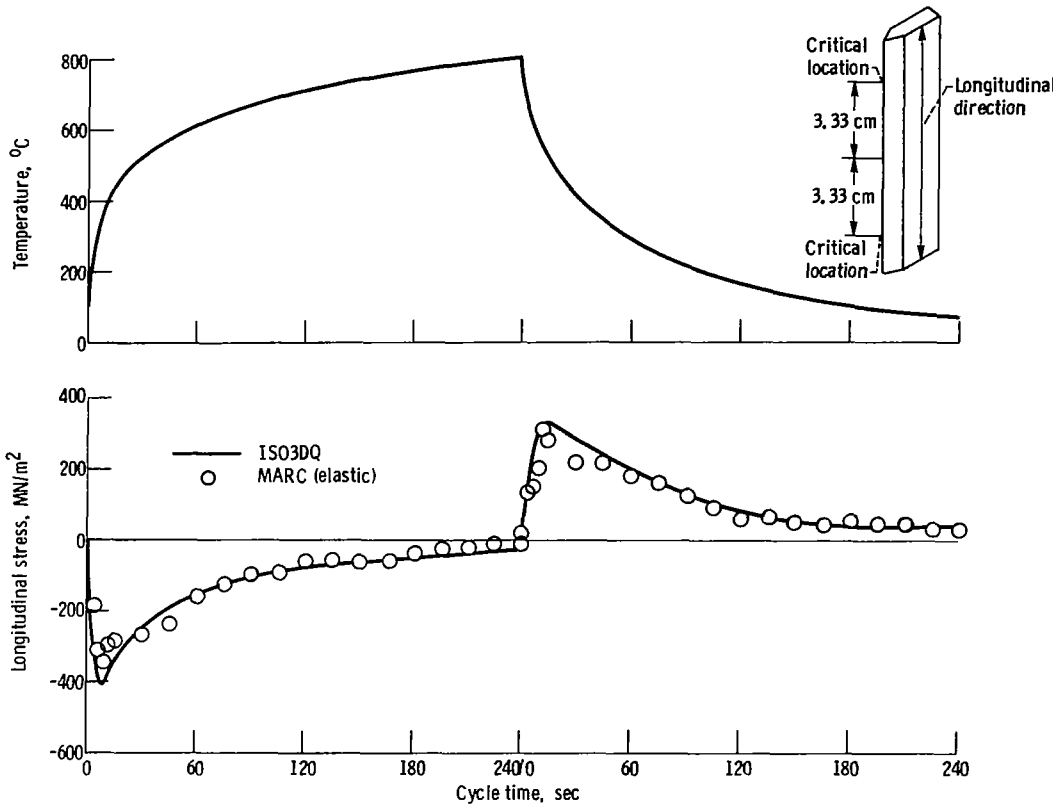

(b) 316 Stainless steel alloy with fluidized beds maintained at 850° and 21° C.

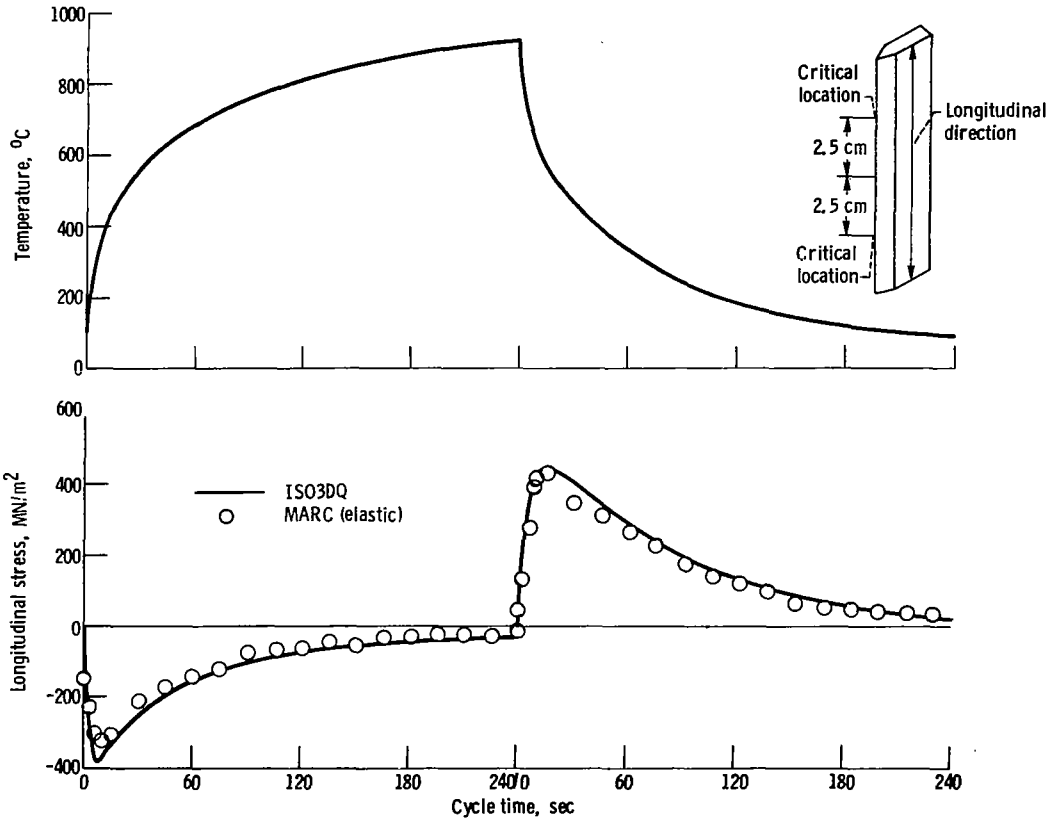

(c) 316 Stainless steel alloy with fluidized beds maintained at 960° and 21° C.

Figure 6. - Concluded.

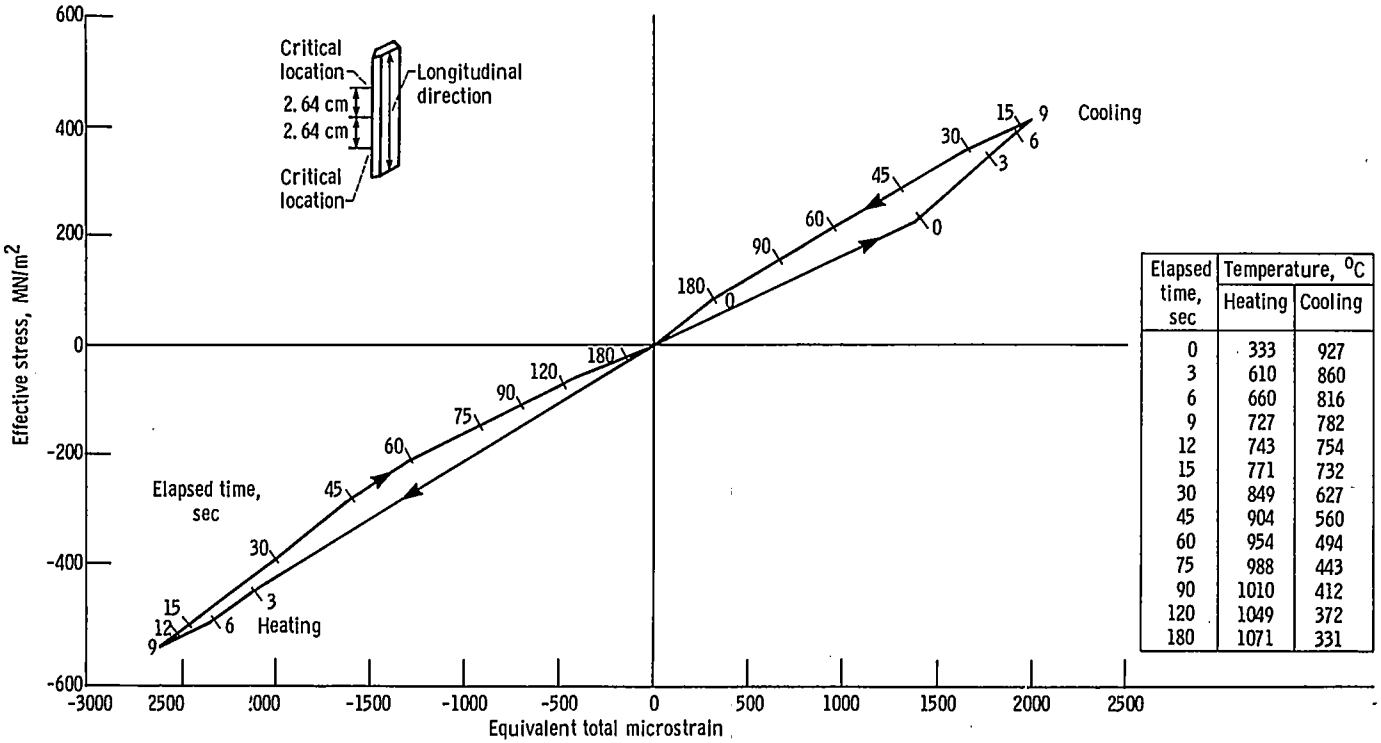

Elapsed time, sec	Temperature, °C	
	Heating	Cooling
0	333	927
3	610	860
6	660	816
9	727	782
12	743	754
15	771	732
30	849	627
45	904	560
60	954	494
75	988	443
90	1010	412
120	1049	372
180	1071	331

(a) NASA TAZ-8A alloy, 1088° C (3 min) - 316° C (3 min).

Figure 7. - Stress-strain response at critical location determined from MARC elastic and elastic-plastic analyses.

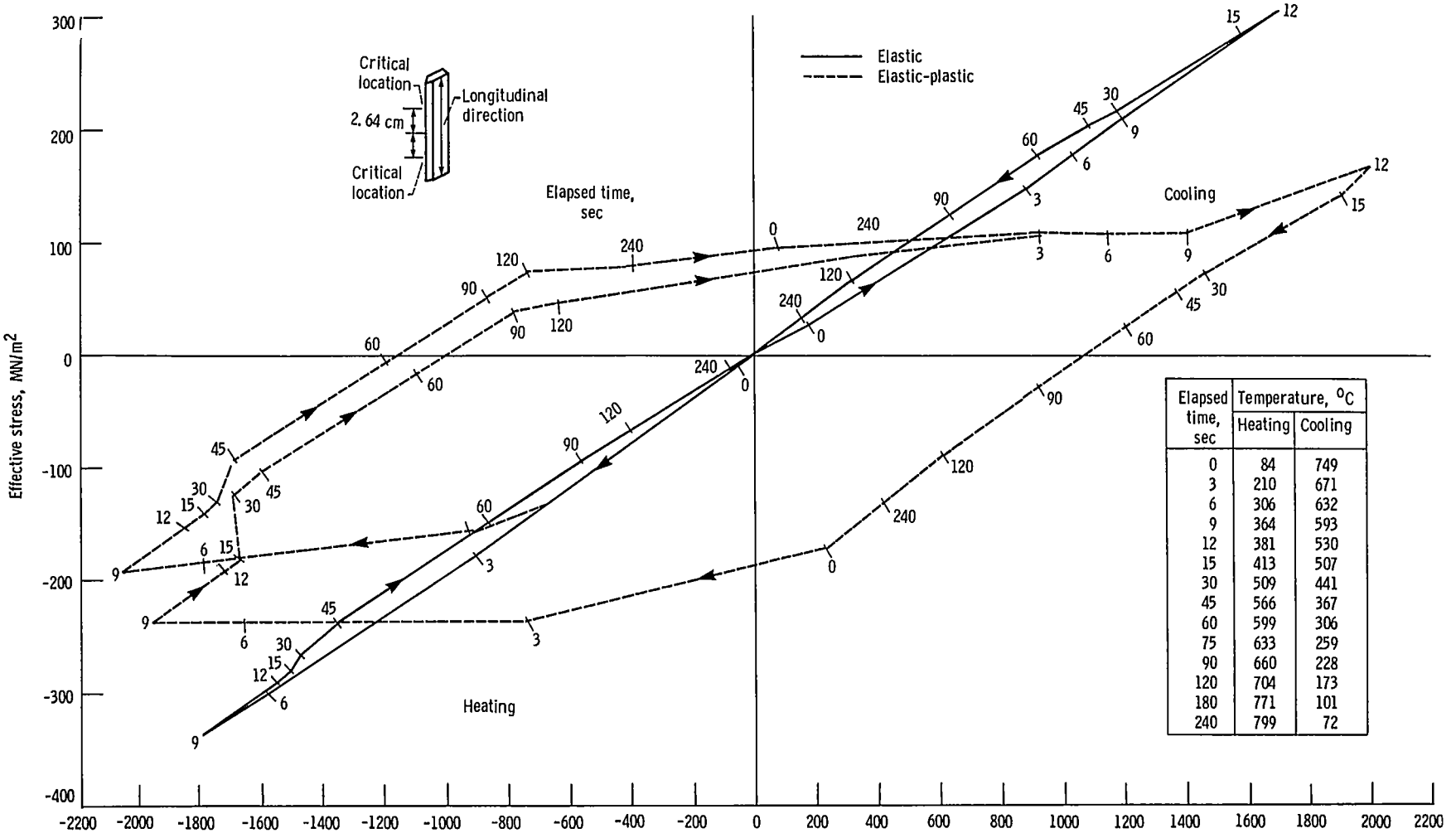

Elapsed time, sec	Temperature, °C	
	Heating	Cooling
0	84	749
3	210	671
6	306	632
9	364	593
12	381	530
15	413	507
30	509	441
45	566	367
60	599	306
75	633	259
90	660	228
120	704	173
180	771	101
240	799	72

(b) 316 Stainless steel alloy, 860° C (4 min) - 21° C (4 min).

Figure 7. - Continued.

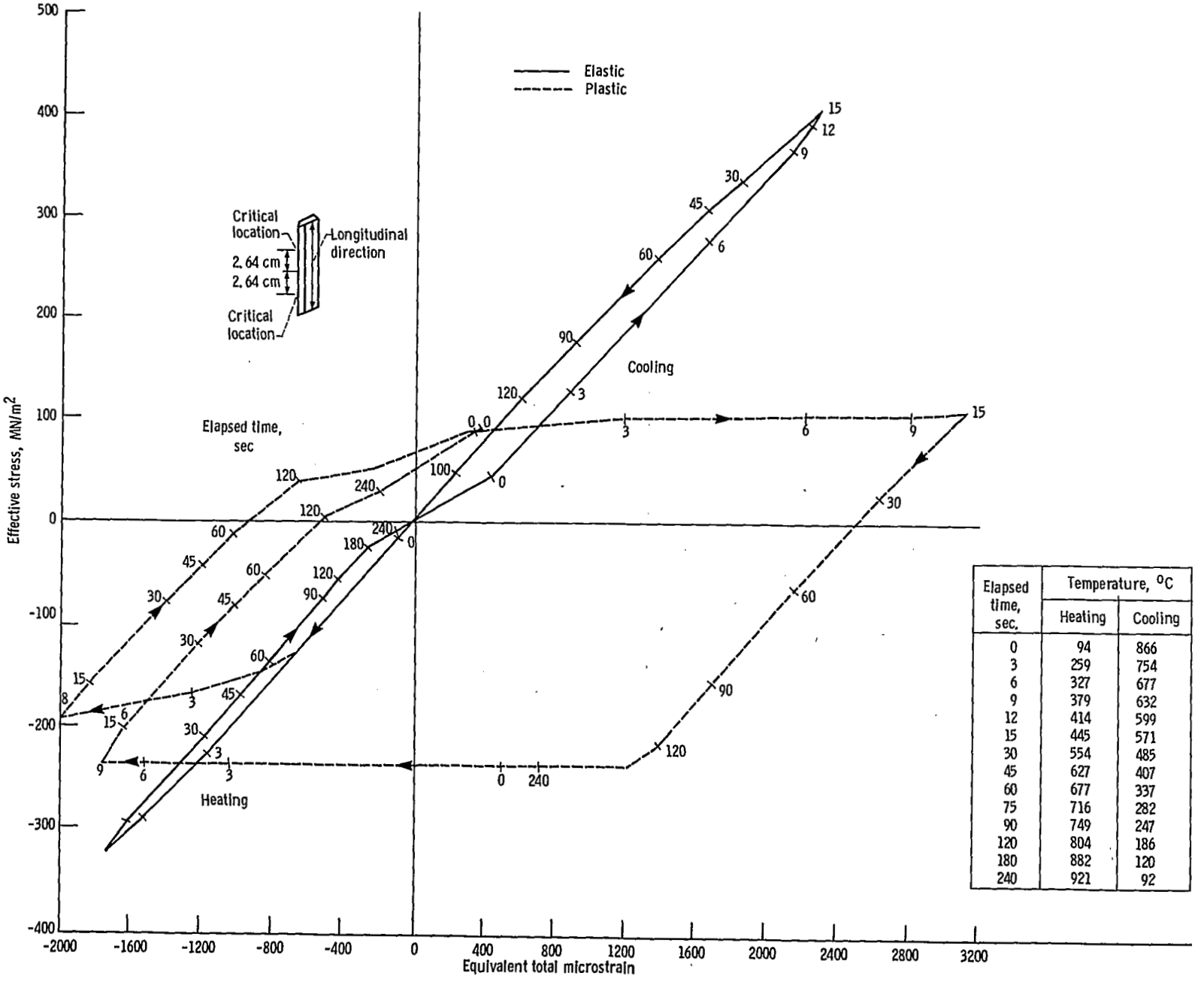

Elapsed time, sec.	Temperature, °C	
	Heating	Cooling
0	94	866
3	259	754
6	327	677
9	379	632
12	414	599
15	445	571
30	554	485
45	627	407
60	677	337
75	716	282
90	749	247
120	804	186
180	882	120
240	921	92

(c) 316 Stainless steel alloy, 960° C (4 min) - 21° C (4 min).

Figure 7. - Concluded.

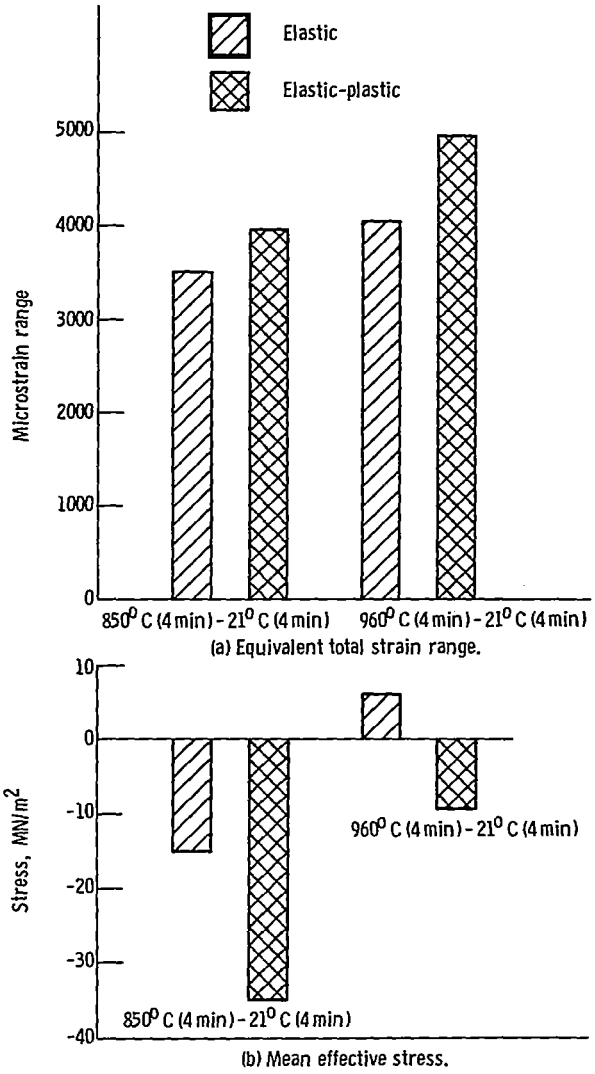

Figure 8. - Comparison of elastic and elastic-plastic (second cycle) analysis results for critical locations of 316 stainless steel alloy specimens.

Contour	Alloy		
	NASA TAZ-8A	316 Stainless steel	
		Low temperature	High temperature
	Temperature, °C		
1	421	131	138
2	463	161	168
3	505	191	198
4	547	220	228
5	589	249	257
6	632	279	287
7	675	309	317
8	718	338	347
9	761	365	376
10	798	397	406

Contour	Alloy		
	NASA TAZ-8A	316 Stainless steel	
		Low temperature	High temperature
	Temperature, °C		
1	32	19	13
2	91	38	38
3	150	57	64
4	209	77	89
5	268	96	115
6	327	115	140
7	386	134	166
8	445	154	191
9	504	173	217
10	563	192	242

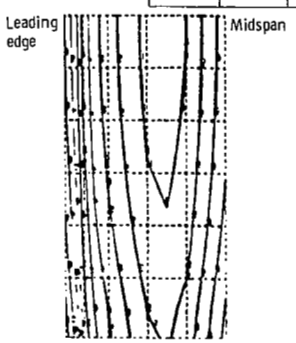

(a-1) NASA TAZ-8A, 9 seconds heating.

(a-2) 316 Stainless steel (low temperature), 9 seconds heating.

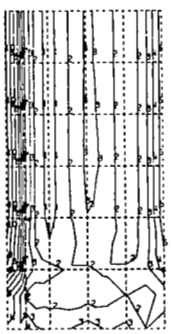

(b-1) NASA TAZ-8A, 9 seconds heating.

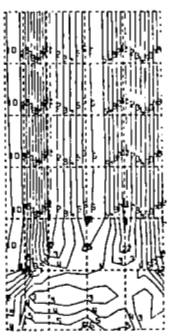

(b-2) 316 Stainless steel (low temperature), 9 seconds heating.

(a-3) 316 Stainless steel (high temperature), 9 seconds heating.

(a) Temperature.

(b-3) 316 Stainless steel (high temperature), 9 seconds heating.

(b) Effective stress.

Figure 9. - Temperature-stress-strain distributions along midchord plane at time of minimum total strain during second cycle.

Contour	Alloy		
	NASA TAZ-8A	316 Stainless steel	
		Low temperature	High temperature
	Temperature, °C		
1	-598	-201	-247
2	-517	-166	-206
3	-436	-132	-165
4	-356	-98	-123
5	-275	-64	-82
6	-194	-30	-40
7	-113	4	1
8	-32	39	42
9	48	73	84
10	129	107	125

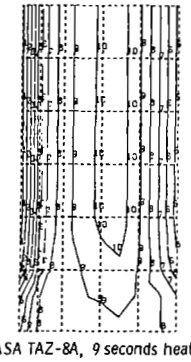

(c-1) NASA TAZ-8A, 9 seconds heating.

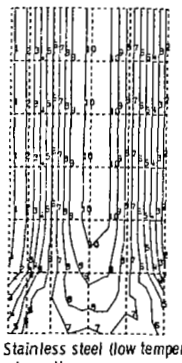

(c-2) 316 Stainless steel (low temperature), 12 seconds cooling.

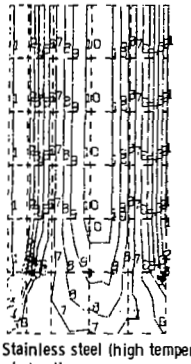

(c-3) 316 Stainless steel (high temperature), 9 seconds heating.

(c) Longitudinal stress.

Contour	Alloy		
	NASA TAZ-8A	316 Stainless steel	
		Low temperature	High temperature
	Temperature, °C		
1	5170	1430	1600
2	5670	1970	2140
3	6170	2500	2680
4	6670	3040	3220
5	7170	3580	3760
6	7670	4110	4300
7	8170	4650	4840
8	8670	5190	5380
9	9170	5720	5920
10	9670	6260	6480

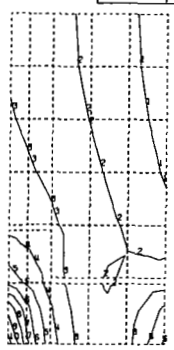

(d-1) NASA TAZ-8A, 9 seconds heating.

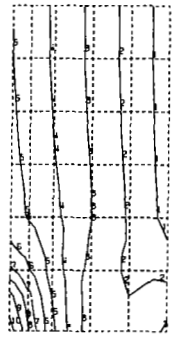

(d-2) 316 Stainless steel (low temperature), 9 seconds heating.

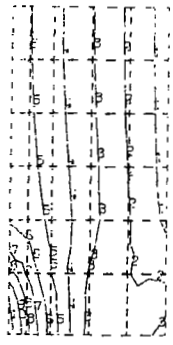

(d-3) 316 Stainless steel (high temperature), 9 seconds heating.

(d) Longitudinal total strain.

Figure 9. - Continued.

Contour	316 Stainless steel alloy	
	Low temperature	High temperature
	Microstrain	
1	60	4
2	177	88
3	295	172
4	412	257
5	529	341
6	647	425
7	764	509
8	881	593
9	999	678
10	1120	762

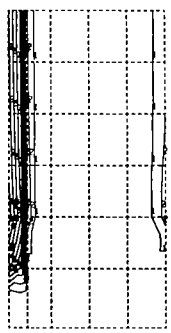

(e-1) 316 Stainless steel (low temperature), 9 seconds heating.

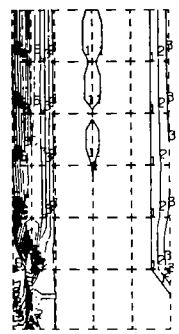

(e-2) 316 Stainless steel (high temperature), 9 seconds heating.

(e) Equivalent plastic strain.

Figure 9. - Concluded.

Contour	Alloy		
	NASA TAZ-8A	316 Stainless steel	
		Low temperature	High temperature
	Temperature, ^{o}C		
1	726	489	510
2	757	512	536
3	787	534	563
4	818	557	590
5	849	579	616
6	880	601	643
7	911	624	669
8	942	647	695
9	973	670	722
10	1004	693	749

Contour	Alloy		
	NASA TAZ-8A	316 Stainless steel	
		Low temperature	High temperature
	Stress, MN/m^2		
1	25	16	6
2	71	36	19
3	117	56	32
4	163	76	45
5	209	96	58
6	255	115	71
7	301	135	84
8	347	155	97
9	393	175	110
10	439	195	123

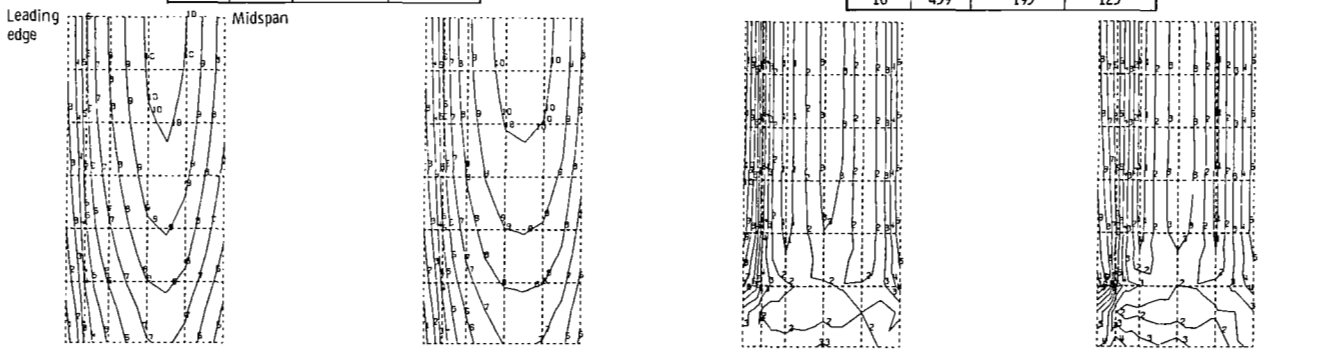

(a-1) NASA TAZ-8A, 9 seconds cooling.

(a-2) 316 Stainless steel (low temperature), 12 seconds cooling.

(b-1) NASA TAZ-8A, 9 seconds cooling.

(b-2) 316 Stainless steel (low temperature), 12 seconds cooling.

(a-3) 316 Stainless steel (high temperature), 15 seconds cooling.

(a) Temperature.

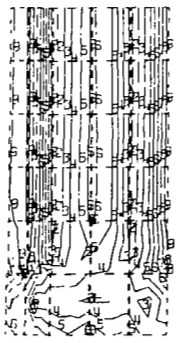

(b-3) 316 Stainless steel (high temperature), 15 seconds cooling.

(b) Effective stress.

Figure 10. - Temperature-stress-strain distributions along midchord plane at time of maximum total strain during second cycle.

Contour	Alloy		
	NASA TAZ-8A	316 Stainless steel	
		Low temperature	High temperature
	Stress, MN/m^2		
1	-106	-50	-63
2	-44	-22	-41
3	18	6	-20
4	80	35	2
5	142	63	23
6	204	91	44
7	266	119	66
8	328	148	87
9	390	177	108
10	452	205	130

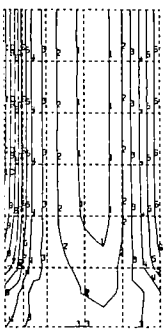

(c-1) NASA TAZ-8A, 9 seconds cooling.

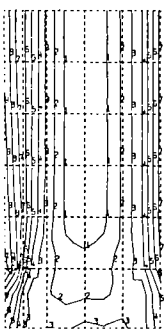

(c-2) 316 Stainless steel (low temperature), 12 seconds cooling.

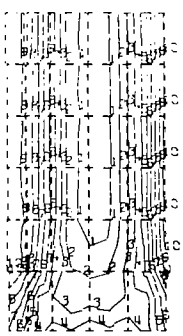

(c-3) 316 Stainless steel (high temperature), 15 seconds cooling.

(c) Longitudinal stress.

Contour	Alloy		
	NASA TAZ-8A	316 Stainless steel	
		Low temperature	High temperature
	Microstrain		
1	9 790	8 850	9 240
2	10 300	9 270	9 710
3	10 800	9 690	10 200
4	11 300	10 100	10 700
5	11 800	10 500	11 100
6	12 400	10 900	11 600
7	12 900	11 400	12 100
8	13 400	11 800	12 600
9	13 900	12 200	13 000
10	14 400	12 600	13 500

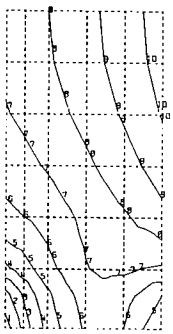

(d-1) NASA TAZ-8A, 9 seconds cooling.

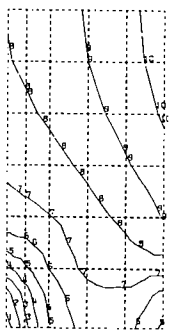

(d-2) 316 Stainless steel (low temperature), 12 seconds cooling.

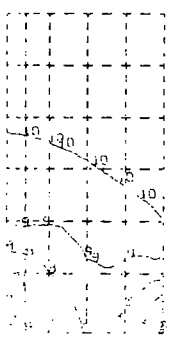

(d-3) 316 Stainless steel (high temperature), 15 seconds cooling.

(d) Longitudinal total strain.

Figure 10. - Continued.

Contour	316 Stainless steel alloy	
	Low temperature	High temperature
	Microstrain	
1	36	88
2	169	368
3	303	647
4	437	926
5	571	1210
6	705	1480
7	839	1760
8	973	2040
9	1110	2320
10	1240	2600

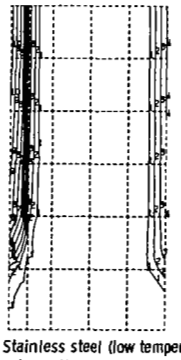

(e-1) 316 Stainless steel (low temperature), 12 seconds cooling.

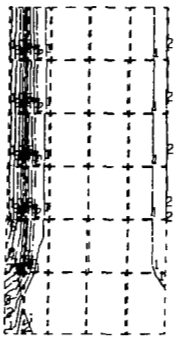

(e-2) 316 Stainless steel (high temperature), 15 seconds cooling.

(e) Equivalent plastic strain.

Figure 10. - Concluded.

1. Report No.	2. Government Accession No.	3. Recipient's Catalog No.
NASA TP-1982		

4. Title and Subtitle	5. Report Date
ELASTIC-PLASTIC FINITE-ELEMENT ANALYSES OF THERMALLY CYCLED SINGLE-EDGE WEDGE SPECIMENS	March 1982
	6. Performing Organization Code 505-33-22
7. Author(s) Albert Kaufman	8. Performing Organization Report No. E-687
9. Performing Organization Name and Address National Aeronautics and Space Administration Lewis Research Center Cleveland, Ohio 44135	10. Work Unit No.
	11. Contract or Grant No.
12. Sponsoring Agency Name and Address National Aeronautics and Space Administration Washington, D. C. 20546	13. Type of Report and Period Covered Technical Paper
	14. Sponsoring Agency Code

15. Supplementary Notes

16. Abstract

Elastic-plastic stress-strain analyses were performed for single-edge wedge alloys subjected to thermal cycling in fluidized beds. Three cases (NASA TAZ-8A alloy under one cycling condition and 316 stainless steel alloy under two cycling conditions) were analyzed by using the MARC nonlinear, finite-element computer program. Elastic solutions from MARC showed good agreement with previously reported solutions that used the NASTRAN and ISO3DQ computer programs. The NASA TAZ-8A case exhibited no plastic strains, and the elastic and elastic-plastic analyses gave identical results. Elastic-plastic analyses of the 316 stainless steel alloy showed plastic strain reversal with a shift of the mean stresses in the compressive direction. The maximum equivalent total strain ranges for these cases were 13 to 22 percent greater than that calculated from elastic analyses.

17. Key Words (Suggested by Author(s))	18. Distribution Statement
Thermal fatigue Structures	Unclassified - unlimited STAR Category 39

19. Security Classif. (of this report)	20. Security Classif. (of this page)	21. No. of Pages	22. Price*
Unclassified	Unclassified	27	A02

* For sale by the National Technical Information Service, Springfield, Virginia 22161

NASA-Langley, 1982